 CMES, vol.87, no.6, pp.483-503, 2012

Functionally Graded Materials (FGMs) with Predictable and Controlled Gradient Profiles: Computational Modelling and Realisation

G. Mattei[1,2], **A. Tirella**[1,2] **and A. Ahluwalia**[1,2]

Abstract: Biological function is intricately linked with structure. Many biological structures are characterised by functional spatially distributed gradients in which each layer has one or more specific functions to perform. Reproducing such structures is challenging, and usually an experimental trial-and-error approach is used. In this paper we investigate how the gravitational sedimentation of discrete solid particles (secondary phase) within a primary fluid phase with a time-varying dynamic viscosity can be used for the realisation of stable and reproducible continuous functionally graded materials (FGMs). Computational models were used to simulate the distribution of a particle phase in a fluid domain. Firstly a model of particle sedimentation was implemented in order to predict the particle gradient profiles. Then the fluid domain was modelled as phase with time dependent viscosity. Experiments were then used to validate the computational results. The models show that selected composition gradients can be tailored by controlling fluid and particle properties. Using this method the gradient of a custom two-phase system can be designed and tailored in a simple fashion. Moreover this approach can also be employed for the fabrication of porous structures, using a porogen as settling particle. The method is particularly useful in tissue engineering applications, to first predict and then control biomaterial gradients without the use of complicated rapid prototyping or computer aided manufacturing systems.

Keywords: Functionally graded materials, computational modelling, sedimentation, tissue engineering, scaffold

[1] Department of Chemical Engineering, Industrial Chemistry and Materials Science, Faculty of Engineering, University of Pisa, Via Diotisalvi, 2 - 56126 Pisa, Italy. Fax: +39 (0)502217866; Tel: +39 (0)502217814

[2] Interdepartmental Research Center "E. Piaggio", Faculty of Engineering, University of Pisa, Via Diotisalvi, 2 - 56126 Pisa, Italy. Fax:+39 (0)502217051; Tel:+39 (0)502217056

1 Introduction

Natural tissues and organs are complex, inhomogeneous structures and most of them are characterised by functional gradients (such as those exhibited by human bone and skin [Ford R.G., Miyamoto Y. and Nogata F. (1999a)]). Depending on its structure, each tissue/organ can possess one or more specific functions. To recapitulate this structure/function relationship, a tissue-engineered scaffold should be graded both in terms of its architecture and mechanical properties. Matching these gradations provides an ideal environment for successful tissue regeneration.

For instance, native articular cartilage exhibits an anisotropic cell distribution from the articular surface to subchondral zone. This distribution is also related to its biomechanical functions. The superficial zone (the one nearest to the articular surface) is the softest, it increases the contact area and distributes the load. The middle and lower zones (the one nearest to the bone) are characterised by minor chondrocyte density and a greater extra-cellular matrix (ECM) secretion, resulting in an increase of the compressive properties from the surface to the deeper zones [Klein T.J., Chaundhry M., Bae W.C. and Sah R.L. (2007)]. More than one cell type is necessary to regenerate multiple tissues, such as bone and cartilage [Sherwood J.K., Riley S.L., Palazzolo R., Brown S.C., Monkhouse D.C., Coates M., Griffith L.G., Landeen L.K. and Ractliffe A. (2002)]. Different cell types means different conditions to preserve their phenotype, hence scaffolds with different features are required. It is well accepted that scaffold pore size, porosity, stiffness and surface properties (i.e. surface composition, surface roughness, topography and hydrophilicity) affect cell morphology and phenotypic expression [Miot S., Woodfield T., Daniels A.U., Suetterlin R., Peterschmitt I., Heberer M., Blitterswijk C.A.V., Riesle J. and Martin I. (2005); Salem A.K., Stevens R., Pearson R.G., Davies M.C., Tendler S.J.B., Roberts C.J., Williams P.M. and Shakesheff K.M. (2002); Sun T., Norton D., Ryan A.J., MacNeil S. and Haycock J.W. (2007)].

Bone tissue is also functionally graded: the outer layer of human bone, or cortical bone, is solid and dense, while the inner layer, cancellous bone, is a spongy honeycombed structure filled with blood vessels and bone marrow maximizing the strength to weight ratio for bending and compression loads. In fact throughout the human body, three-dimensional architectures exhibit spatially varying mechanical properties, and again most of them show a structure/function relationship [Ford R.G., Miyamoto Y. and Nogata F. (1999a)]. An important feature of biological gradients is their continuity. There are no sharp boundaries and no interfaces.

In the world of engineering, spatial gradients can be generally categorised as continuous and discrete gradients [Ford R.G., Miyamoto Y., Rabin B.H. and Williamson R.L. (1999b)]. Discrete gradient materials are multi-layered structures obtained

stacking different homogeneous layers. Their main advantage can be summarised in the fine control of porosity, pore size and composition of each layer. However, discontinuities at the interfaces between layers may affect pore interconnection (with negative effects on cell ingrowth and transport of nutrients and wastes) and can cause delamination between layers due to stress concentration. Continuous FGMs are characterised by a continuous change in their microstructure, and no delamination problems occur in them. However there are few reports on the fabrication of continuous FGMs, and most of them are related to the control of pore distribution. Indeed the mechanical properties of a scaffold can be controlled by varying the porosity and/or pore size across its volume.

Fabrication techniques to manufacture structures with gradients can be divided in conventional and advanced processing methods. Conventional techniques do not have full control of the macro- and micro-architecture; they use porogens as a first step [Werner J., Linner-Krcmar B., Friess W. and Greil P. (2002)] and fillers to glue the layers (such as cellulose sponges and hydroxyapatite (HA) slurries [Tampieri A., Celotti G., Sprio S., Delcogliano A., Franzese S. (2001)]). New approaches such as self-foaming followed by pyrolysis [Zeschky J., Hofner T., Arnold C., Weissmann R., BahloulHourlier D., Scheffler M. and Greil P. (2005)] or centrifugation methods [Oh S.H., Park I.K., Kim J.M. and Lee J.H. (2007)] can be used to fabricate scaffolds with continuous gradients, but there is no control over the gradient obtained.

Besides the previously mentioned techniques, advanced processing methods use computer-aided design (CAD) and rapid prototyping (RP) techniques to fabricate structures with discrete and semi-continuous gradients. Hollister et al. showed that scaffolds of a given material (with known Young's modulus and Poisson's ratio) and a certain 3D shape could match the stiffness or strength of natural tissues [Hollister, S. J. (2005); Hollister, S. J., Maddox, R. D. and Taboas, J. M. (2002); Adachi, T., Osako, Y., Tanaka, M., Hojo, M. and Hollister, S. J. (2006)]. In this way, modelling scaffold shape, pore size, porosity and material enables prediction of its overall mechanical response. CAD modelling used in conjunction with RP techniques to manufacture a totally controllable structure is particularly useful for TE applications, allowing optimal reproducibility over many kinds of 3D shapes and materials. Moreover it is possible to design a scaffold mimicking an anatomical structure to be replaced [Van Cleynenbreugel, T., Van Oosterwyck, H., Vander Sloten, J. & Schrooten, J. (2002); Hutchmacher, D. W. & Cool, S. (2007); Smith, M. H., Flanagan, C. L., Kemppainen, J. M., Sack, J. A., Chung, H., Das, S., Hollister, S. J. & Feinberg, S. E. (2007)]. RP methods were used to produce structures with discrete gradients (e.g. FDM [Kalita S.J., Bose S., Bandyopadhyay A. and Hosick, H.L. (2003)], 3D Fiber Deposition [Woodfield T.B.F., Malda J.,

de Wijn J., Peters F., Riesle J. and van Blitterswijk C.A. (2004)], PAM [Vozzi G. and Ahluwalia A. (2007)], PAM2 [Tirella A., Vozzi F., Vozzi G. and Ahluwalia A. (2011)]) and semi-continuous gradients (e.g. TheriformTM [Sherwood J.K., Riley S.L., Palazzolo R., Brown S.C., Monkhouse D.C., Coates M., Griffith L.G., Landeen L.K. and Ractliffe A. (2002)]). It is still a challenge to develop suitable computer aided systems to design and manufacture continuous FGM.

To overcome these problems, here we propose a method to realise continuous FGM using gravitational sedimentation of discrete solid particles (i.e. hydroxyapatite) within a primary fluid phase. A time-varying dynamic viscosity fluid phase (i.e. gelatin solution) is used to fix a gradient with a controlled gradient profile. After establishing the properties of the materials used (such as particle size, fluid properties, etc.), a computational fluid dynamic (CFD) model was used to overcome the trial-and-error experimental approach generally used to obtain continuous gradients. After solving the CFD model, the results obtained were used to set-up the experimental conditions necessary to obtain the desired granular phase gradient (such as sedimentation time, gelation of the fluid phase, particle dimensions). To verify the computational model, a simple two-phase sedimentation system (primary fluid phase with constant dynamic viscosity) was solved and experimentally validated. Then, a more complex system was modelled introducing the time-variance of dynamic viscosity of the primary phase (i.e. sol-gel transition). Gelatin solutions were used as the primary phase, and thermal gelation used to control the dynamic viscosity as function of temperature. The latter model can be used to predict and tailor particle gradients by controlling the viscosity of the primary phase as function of time, or temperature. This novel approach can be used to first design and then fabricate complex structures with biologically and physiologically relevant gradients for TE applications.

2 Computational modelling

The sedimentation process of solid particles (secondary phase) in fluids (primary phase), respectively having different diameters and viscosities, was numerically modeled using commercial CFD software (ANSYS FLUENT). The interaction between particles and fluid, as well as its viscosity, were considered. The Eulerian multiphase model was used to model multiple separate interacting phases (solid and liquid phases): a single pressure shared by all phases, while momentum and continuity equations solved for each phase separately. Moreover, solid-phase stresses were derived making an analogy between the random particle motion (arising from particle-particle collisions) and the thermal motion of molecules in a gas: the intensity of the particle velocity fluctuations determines the stresses, viscosity, and pressure of the solid phase [Ding J. and Gidaspow D. (1990); Lun C. K. K., Sav-

age S. B., Jeffrey D. J., and Chepurniy N. (1984); Syamlal M., Rogers W., and O'Brien T. J. (1993)]. In the model we assume that the kinetic energy associated with the particle velocity fluctuations is represented by a "pseudo-thermal" or granular temperature (which is proportional to the mean square of the random motion of particles).

2.1 Fundamental equations

Fundamental equations used to solve the model are presented below in their general form. Symbols are listed in the Nomenclature section. In the adopted notation $\boldsymbol{q}$ refers to the analysed phase, while $\boldsymbol{p}$ represents one of the n phases of the model.

2.1.1 Continuity equation

The continuity equation (conservation of mass) for a phase $\boldsymbol{q}$ is:

$$\frac{\partial}{\partial t}(\alpha_q \rho_q) + \nabla \cdot (\alpha_q \rho_q \vec{v}_q) = \sum_{p=1}^{n} (\dot{m}_{pq} - \dot{m}_{qp}) + S_q \tag{1}$$

In case of simple particle sedimentation (i.e. no mass transfer and no sources) both mass transfer terms ($\dot{m}_{pq}$ and $\dot{m}_{qp}$) and source term S_q are null within the model. For this reason they were not considered futher.

2.1.2 Momentum equation

The momentum balance for a phase $\boldsymbol{q}$ can be expressed as:

$$\begin{aligned} &\tfrac{\partial}{\partial t}(\alpha_q \rho_q \vec{v}_q) + \nabla \cdot (\alpha_q \rho_q \vec{v}_q \vec{v}_q) = -\alpha_q \nabla p + \nabla \cdot \bar{\bar{\tau}}_q + \alpha_q \rho_q \vec{g} + \\ &\sum_{p=1}^{n} (\vec{R}_{pq} + \dot{m}_{pq} \vec{v}_{pq} - \dot{m}_{qp} \vec{v}_{qp}) + (\vec{F}_q + \vec{F}_{lift,q} + \vec{F}_{vm,q}) \end{aligned} \tag{2}$$

$$\bar{\bar{\tau}}_q = \alpha_q \mu_q (\nabla \vec{v}_q + \nabla \vec{v}_q^T) + \alpha_q (\lambda_q - \frac{2}{3} \mu_q) \nabla \cdot \vec{v}_q \bar{\bar{I}} \tag{3}$$

In Eq. 2 $\bar{\bar{\tau}}_q$ is the $\boldsymbol{q}^{th}$ phase stress tensor and $\vec{v}_{pq}$ is the interphase velocity, respectively defined in Eq. 3 or related to the mass transfer term $\dot{m}_{pq}$. In particular the interphase velocity is a null term.

It should be considered that the lift force acts on a particle mainly due to velocity gradients in the primary-phase flow field and is more relevant in case of larger particles. Since it is rather insignificant compared to the drag force, the term $\vec{F}_{lift,q}$ in Eq. 2 was not included in the computational model. Moreover it has to be taken into account that, when a secondary phase $\boldsymbol{p}$ accelerates relative to the primary fluid phase $\boldsymbol{q}$, the inertia of the primary-phase mass encountered by accelerating particles exerts a *virtual mass force* on the particles, represented by $\vec{F}_{vm,q}$ in Eq. 2.

This effect, called *virtual mass effect* (VME), is significant only when the secondary phase density is much smaller than the primary phase density, so it was neglected in the model.

The interphase force ($\vec{R}_{pq}$ in Eq. 2) depends primarily on the friction, the pressure and the cohesion, and is subject to the conditions that $\vec{R}_{pq} = -\vec{R}_{qp}$ and $\vec{R}_{qq} = 0$. ANSYS FLUENT models this force using a simple interaction (Eq. 4), in which $K_{pq}(=K_{qp})$ represents the interphase momentum exchange coefficient (in granular flows, the momentum exchange between phases depends on fluid-fluid, fluid-solid and solid-solid exchange coefficients respectively expressed as K_{ll}, K_{sl} and K_{ss}). The modelled system consists only of a primary liquid phase and a secondary granular phase; again another term (namely the fluid-fluid exchange coefficient) can be neglected. In the fluid-solid exchange coefficient (Eq. 5) the coefficient f includes a drag function (C_D), which depends on the relative Reynolds number (Re_s) and differs according to the model chosen to represent the exchange coefficient.

$$\sum_{p=1}^{n} \vec{R}_{pq} = \sum_{p=1}^{n} K_{pq}(\vec{v}_p - \vec{v}_q) \tag{4}$$

$$K_{sl} = \frac{\alpha_s \rho_s f}{\tau_s} \tag{5}$$

We followed the Syamlal-O'Brien approach [Syamlal M. and O'Brien T. J. (1989)] defining f as expressed in Eq. 6a, in which the drag function is modelled as Dalla Valle [Dalla Valle J. M. (1948)] (Eq. 6b). The Syamlal-O'Brien model is based on measurements of particle terminal velocities in settling beds, with correlations that are a function of volume fraction and Re_s [Richardson J. R. and Zaki W. N. (1954)]. In particular the Re_s, expressed in Eq. 6c, takes into account the l^{th} fluid phase and the s^{th} solid phase. In Eq. 6c the terminal velocity correlation for the solid phase $v_{r,s}$ is defined according to Garside and Al-Dibouni [Garside J. and Al-Dibouni M. R. (1977)]. To complete this scheme, the term τ_s (expressed in Eq. 5) is the *particulate relaxation time* defined in Eq. 7.

$$f = \frac{C_D Re_s \alpha_l}{24 v_{r,s}^2} \tag{6a}$$

$$C_D = \left(0.63 + \frac{4.8}{\sqrt{Re_s / v_{r,s}}}\right)^2 \tag{6b}$$

$$Re_s = \frac{\rho_l d_s \left|\vec{v}_s - \vec{v}_l\right|}{\mu_l} \tag{6c}$$

$$\tau_s = \frac{\rho_s d_s^2}{18 \mu_l} \tag{7}$$

Finally, the solid-solid exchange coefficient among particles, has been modelled following the form proposed by Syamlal et al. [Syamlal M. (1987)] as shown in Eq. 8, in which the friction coefficient $C_{fr,ls}$ between the l^{th} and s^{th} solid-phase particles is zero.

$$K_{ls} = \frac{3\,(1+e_{ls})\left(\frac{\pi}{2}+C_{fr,ls}\frac{\pi^2}{8}\right)}{2\pi(\rho_l d_l^3+\rho_s d_s^3)} \cdot \alpha_s\rho_s\alpha_l\rho_l\,(d_l+d_s)^2\,g_{0,ls}\,|\vec{v}_l-\vec{v}_s| \tag{8}$$

2.2 Setting up the model

The sedimentation of the granular phase (which is initially evenly dispersed within the liquid phase) was numerically simulated using the Eulerian model of the Euler-Euler methods. As stated before, the Syamlal-O'Brien model was chosen to describe the interaction between phases.

2.2.1 Solids Pressure

For granular flow in the compressible regime (which means solid volume fraction less than its maximum allowed value), a solids pressure term is calculated independently and used as pressure gradient term in the granular-phase momentum equation. The solids pressure is composed of a kinetic term and a second term due to particle collisions. The Lun et al. formulation (default settings in ANSYS FLUENT) was chosen to compute solids pressure in this model.

2.2.2 Radial distribution function

The radial distribution function $g_{0,ss}$ is a correction factor that modifies the probability of collisions between particles when the solid granular phase becomes dense (transition from the compressible condition, $\alpha < \alpha_{s,\max}$, to the incompressible condition, $\alpha = \alpha_{s,\max}$). Since our sedimentation problem involves a single solid phase, the formulation proposed by Lun et al. was chosen for $g_{0,ss}$ [Ogawa S., Umemura A., and Oshima N. (1980)].

2.2.3 Packing limit

The packing limit is an important empirical parameter used to characterise the maximum volume fraction of randomly packed solid objects. It does not have a precise geometric definition and depends theoretically on the number and the diameter of particles dispersed within a given volume. If the system has poly-dispersed particles, the small ones accumulate in between larger particles increasing the packing limit, which depends non-trivially on the size-distribution and can be close to 1. The volume fraction for mono-disperse spherical objects in random close packing

cannot exceed a density limit of 0.634 [Song C., Wang P. and Makse H.A. (2008)], while a very loose random packing model with a packing limit of 0.56 is appropriate for slowly settling spheres [Dullien F.A.L. (1992)]. In this work the packing limit was experimentally derived, and the resulting value was then used in the CFD model.

2.2.4 Solids shear stresses

The solid stress tensor contains shear and bulk viscosities arising from particles momentum exchange (which is due to translation and collision). The solid shear viscosity is the sum of collisional, kinetic and frictional components. Here the collisional part was modelled according to Syamlal et al. [Syamlal M., Rogers W., and O'Brien T. J. (1993)], while the Syamlal-O'Brien expression was chosen for the kinetic part. The frictional component was neglected in the numerical model, since it accounts for the generation of frictional stresses between particles (relevant only in dense flow at low shear). The solids bulk viscosity accounts for the resistance of the granular particles to compression and expansion and here takes the Lun et al. form [Lun C. K. K., Savage S. B., Jeffrey D. J., and Chepurniy N. (1984)].

2.2.5 Granular temperature

As anticipated, the granular temperature for the s^{th} solid phase is proportional to the kinetic energy of the random motion of the particles. The transport equation derived from kinetic theory takes the form presented by Ding and Gidaspow [Ding J. and Gidaspow D. (1990)]. An algebraic formulation (default settings in ANSYS FLUENT) was used to solve the granular temperature, and thus convection and diffusion were neglected in the transport equation.

2.2.6 Other settings

Surface tension between fluid and granular solid phase were neglected in the model. Since the gravitational sedimentation is relatively slow (very low Reynolds number), no turbulence models were considered. Therefore a laminar model was chosen.

3 Experiments

The main objective of the experiments was to validate the CFD models. Particle distribution was monitored during the sedimentation of evenly dispersed microparticles in a fluid media. Since the aim is to obtain continuous FGM, the gravitational sedimentation of discrete solid particles within a time-varying primary viscous fluid phase was analysed. As first step, a two-phase sedimentation CFD model

was developed considering a primary fluid phase with constant dynamic viscosity. Glucose micro particles (G7021, Sigma-Aldrich, sieved to obtain particles between 88 and 105 μm) suspended in commercial olive oil were used to experimentally validate this model. Secondly the model was modified introducing a time-varying dynamic viscosity condition to the primary phase. HA (21223, Sigma-Aldrich, mean diameter 20 μm measured using a microscope) homogeneously suspended in a gelatin solution were used in the experimental model. The time-varying behaviour of gelatin dynamic viscosity during its gelation process was first measured experimentally and then fitted to an empirical function, leading to the prediction of the final particle gradient when gelatin completes the physical gelation. A purposely made polydimethylsiloxane (PDMS) "U-shaped" mold (which we named Usystem) was designed to hold two 3x1" microscope glass slides, and used in the experimental part. In this way it was possible to monitor a known volume of suspension during particle sedimentation (Fig. 1).

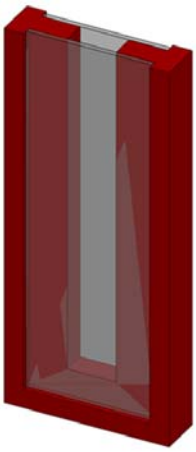

Figure 1: The Usystem or PDMS mold (red) holding 3x1" microscope glass slides. The device was purposely designed to house a known volume of particle suspension and to easily monitor the sedimentation process.

3.1 Constant viscosity system

Glucose particles (density, 1540 kg/m^3; average diameter, 100 μm) were left to settle into oil (density, 920 kg/m^3; viscosity, 0.084 Pa•s). The mixture was prepared using 569 mg of glucose particles, adding oil to reach a final volume of 10 mL. Particles were evenly dispersed within the primary fluid phase using a vortex mixer, obtaining a homogeneous particle volume fraction of 0.037. Then, 1.8 mL was put

into the Usystem (sedimentation volume of 12x5x30 mm^3). To monitor particle sedimentation, pictures were taken at known time intervals using a camera (Canon EOS 60D) (Fig. 2). One important parameter measured during the experiments was the settling time. The settling time is the time necessary to reach the steady state in which no change occurs in particle concentration. The experimental average settling time was about 30 minutes.

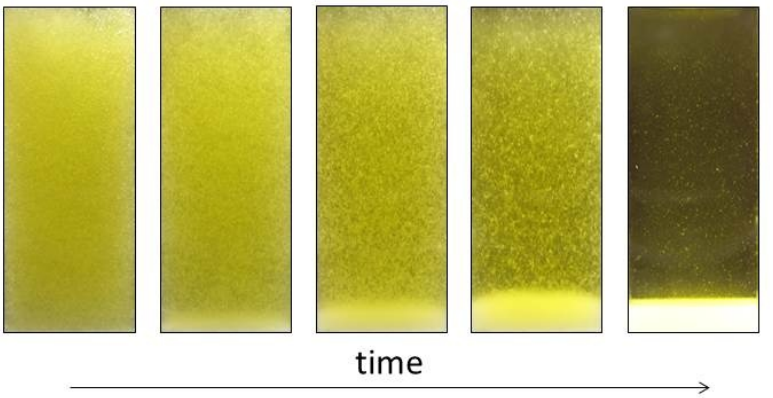

Figure 2: Details of the sedimentation process at different time intervals. As sedimentation occurs, particles (secondary phase) are easily visible at the bottom of the system.

3.2 Time-varying viscosity system

Continuous FGM were obtained using the gravitational sedimentation of HA microparticles and a gelatin solution in a temperature controlled system. A 5% w/v gelatin solution was prepared dissolving type A gelatin (Gelatin from porcine skin, G2500 - Type A, Sigma Aldrich) in a 1x phosphate buffered solution (PBS, Sigma-Aldrich). Then HA particles (density, 3157 kg/m^3; average diameter, 20 μm) were added to the gelatin solution to obtain a solid volume fraction of 0.037. The mixture was stirred at 37 ˚C until particles were evenly suspended. Then 1.8 mL of homogeneous gelatin-HA suspension was transferred into the Usystem. In order to obtain a continuous gradient, the sedimentation was performed at 10 ˚C. This temperature guarantees a quick physical gelation of gelatin solution in the Usystem, preventing the complete settling of HA particles and at the same time preventing a too rapid gelation of the primary phase, which does not allow the settling of HA particles at all (Fig. 3). Once the gelation occurs, the particle graded hydrogels were easily removed from the Usystem by unclamping the two microscope slides.

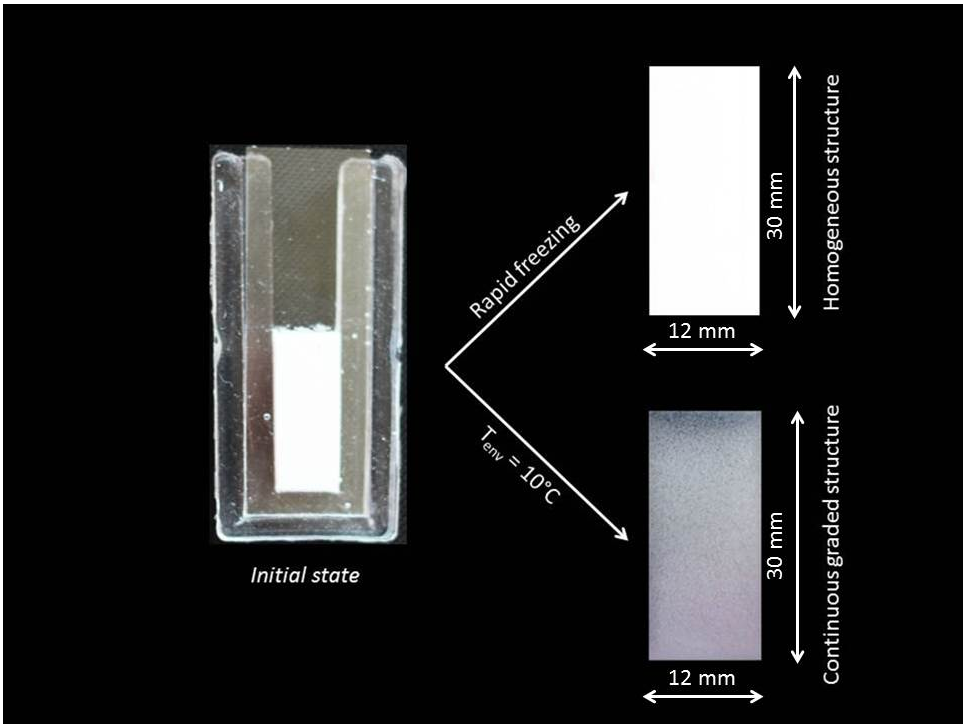

Figure 3: Sedimentation of HA particles within gelatin at 10 Â°C and rapid freezing. The gelation time should be of the same order as the sedimentation time, otherwise particles pack at the bottom of the system (no gelation) or are homogeneously suspended (rapid freezing). Intermediate temperatures can be used to control the sedimentation process and thus obtain controlled particle gradients.

4 CFD model validation: results and discussion

The particle settling process was computationally simulated solving a 3D time-dependent sedimentation model in ANSYS FLUENT. The studied sedimentation system was modelled as the Usystem domain and then meshed using a regular cubic grid with 14400 cells. The stationary wall boundary condition was chosen for all boundaries (i.e. the external surface of the modelled volume). The maximum packing limit was experimentally determined (i.e. 0.5) and used in the model. The initial volume fraction considered for the solution was the same one used in experiments (i.e. 0.037). The model takes into account particle inertia and other aspects (e.g. collisions between particles, changes in local effective viscosity due to particle settling, etc.) that can modify particle motion with respect to the ideal situation

of non-interacting particles (very low particle volume fractions). Stoke's equation (eq. 9) is generally used to derive particle settling velocity in ideal conditions, i.e. in the absence of particle-particle interaction.

$$v_0 = \frac{2(\rho_p - \rho_f) g r^2}{9\mu} \tag{9}$$

where v_0 is the settling velocity, ρ_p is the glucose density, g is the acceleration due to gravity, r is the glucose particle radius and μ is the dynamic viscosity of the oil.

In concentrated suspensions, particles interact during sedimentation and then both the hydrodynamic interaction between particles and other higher order interactions should be considered. To further validate the CFD model results, we used Batchelor's theory [Batchelor G.K. (1972)] for sedimentation in a relatively dilute dispersion of spheres (volume fraction up to 0.1). In this theory, settling velocity is influenced by particle number: a reduction of nominal Stoke's velocity is associated with increasing particle number.

The mean value of the velocity of a sphere can be calculated as expressed by Eq. 10, where ϕ is particle volume fraction and v_0 is the velocity of a single sphere in unbounded fluid (i.e. Stokes' velocity). At higher volume fractions, the sedimentation velocity becomes a complex function of ϕ and only empirical equations are available to describe the variation of v with ϕ.

$$v = v_0(1 - 6.55\phi) \tag{10}$$

4.1 Particles settling in a fluid phase with constant viscosity: validating the CFD model

Material properties (i.e. oil density and viscosity, glucose particles density and diameter) were defined in the simple two-phase sedimentation model considering a primary fluid phase with constant dynamic viscosity (see section 3.1 for physical values). The Stokes' velocity for the studied system is $4.02 \bullet 10^{-5}$ m/s,

The settling velocity of a sphere in a suspension with a particle volume fraction of 0.037 can be calculated from the Stokes' velocity using the equation proposed by Batchelor (eq. 9). The resultant value of $3.04 \bullet 10^{-5}$ m/s can be compared with the mean velocity of the solved CFD model in the first settling instants (i.e. particle volume fraction is homogeneous and similar to 0.037), which was found to be equal to $3.09 \bullet 10^{-5}$ m/s. Since no a priori assumptions were made about the settling velocity, this result contributes to prove the validity of the proposed model.

The solution of the time-dependent CFD sedimentation model at different times is shown in Fig. 4. Snapshots of the corresponding experimental results are shown in the same figure for ease of comparison. Particles rapidly leave the top of the domain

and settle to the bottom, increasing their volume fraction. The solution of the model showed no more changes in particle concentration after 30 minutes. Thus, the settling time needed to reach the steady state was the same as the experiments, further confirming the validity of the model. Moreover two regions separated by a step discontinuity can be distinguished at the end of the sedimentation process: a suspension with a concentration equal to the maximum packing limit (i.e. 0.5) and a layer of clear oil on the top.

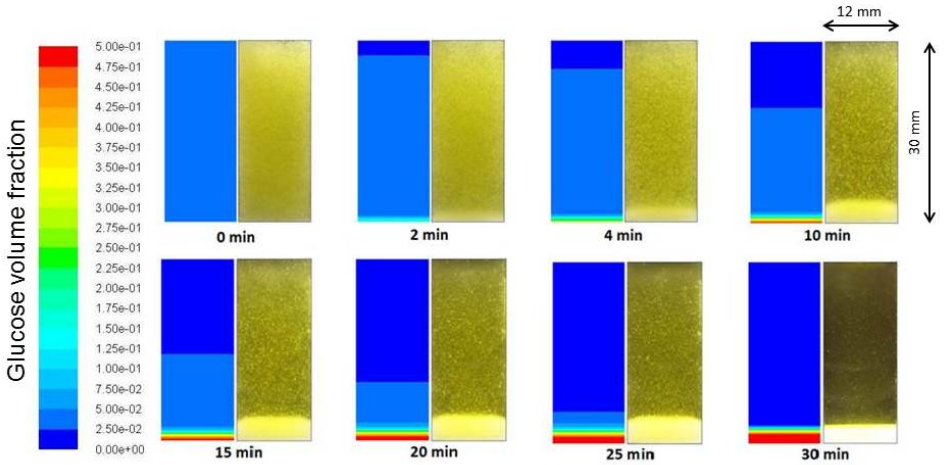

Figure 4: Comparison between CFD solutions (glucose volume fraction) and the corresponding experimental results at different times of the settling process.

4.2 Modeling particle sedimentation in a time-varying primary fluid phase to obtain continuous FGM

The gravitational sedimentation of micro-particles within a viscous phase (characterised by a time/temperature-varying dynamic viscosity) was modelled and experimentally validated to obtain stable continuous FGM. A CFD model was implemented in order to predict and control particle gradient profiles within FGMs. The time-dependence of gelatin viscosity as function of temperature was derived in the studied system as follows: dynamic viscosity (μ) was measured using a rotational rheometer (Physica Rheolab MC 20 with concentric cylinders configuration) as function of temperature (T). An exponential decay function was used to fit the collected data (Fig. 5), obtaining Eq. 11 to describe μ as a function of T.

$$\mu(T) = 0.00559 + 4.76601 \cdot 10^{11} \cdot e^{-T/0.89429} \tag{11}$$

Viscosity data above 40 ˚C were not represented as the gelatin solution viscosity does not significantly change: below the gelation point (26 ˚C) the material tends to a solid phase.

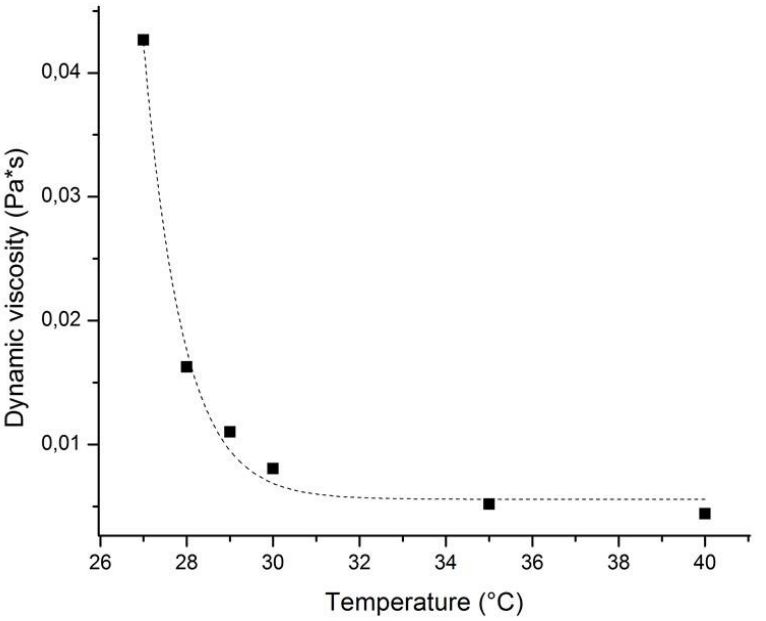

Figure 5: Dynamic viscosity of gelatin as a function of temperature. Experimental data (squares) and resulting fitting (dashed line); R^2=0.989

At this point the temperature time-behaviour of the gelatin solution in the Usystem (Fig. 1) was measured using a temperature sensor. Collected data were fitted using an empirical exponential decay function (Fig. 6), and finally the temperature time-behaviour of the gelatin solution in the studied system was obtained (Eq. 12).

$$T(t) = 10.3 + 27.1 \cdot e^{-0.0033t} \tag{12}$$

The time-dependence of gelatin viscosity was extrapolated combining Eq. 11 and 12 to Eq. 13.

$$\mu(t) = 0.00559 + 4.76601 \cdot 10^{11} \cdot e^{(-(10.3+27.1 \cdot e^{-0.0033t})/0.89429)} \tag{13}$$

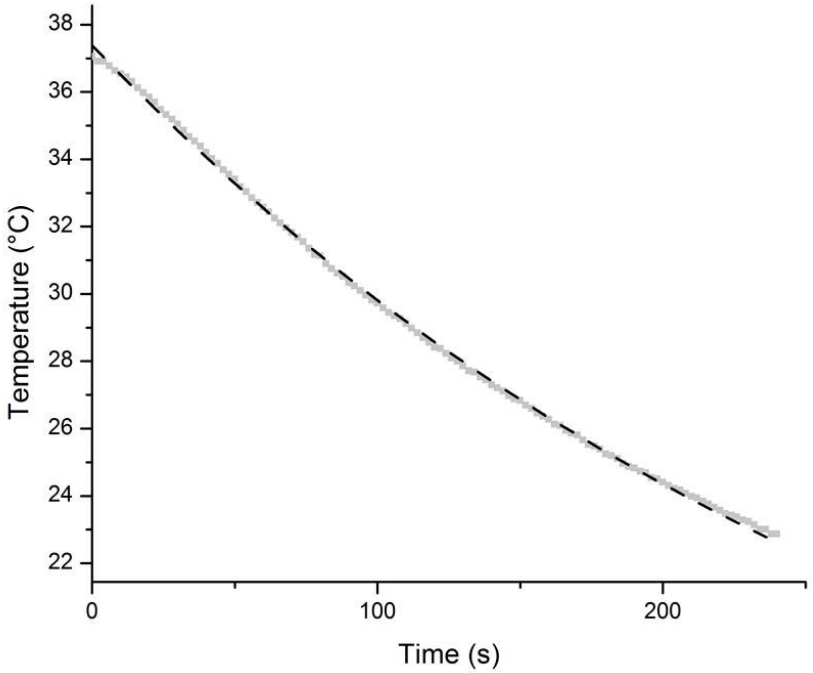

Figure 6: Temperature of gelatin solution in the presented system as function of time. Experimental data (squares) and resulting fitting (dashed line); R^2=0.999.

To model the time-dependence of gelatin viscosity during its gelation process in the Usystem in ANSYS FLUENT, Eq. 13 was implemented using a custom UDF (User Defined Function). The density of the primary fluid phase (i.e. 5% w/v gelatin solution in PBS) was calculated using the following formula:

$$\rho_{solution} = 0.05 \cdot \rho_{gelatin} + 0.95 \cdot \rho_{PBS} = 1.0175 \frac{g}{cm^3} \tag{14}$$

In Eq. 14 $\rho_{gelatin}$ is 1.35 g/cm^3 [Fels IG. (1964)] and ρ_{PBS} is approximated to be the one of water.

In the Usystem 150 seconds are required to complete the gelation and stop HA sedimentation. Fig. 7 shows the HA particle gradient obtained within the gelatin primary phase, while in Fig 8 a comparison between the CFD model and experimental results is shown. Note that there are no discontinuities within the composition gradient. Furthermore, as demonstration of a stable FGM, solving the CFD sedimentation model for longer times (e.g. 200 seconds) does not change the par-

ticle gradient (which remains equal to the one obtained after 150s). In fact, the fraction does not change with time after the gelation point is reached, resulting in a well-defined composition gradient within the realised scaffold, in agreement with the experimental results.

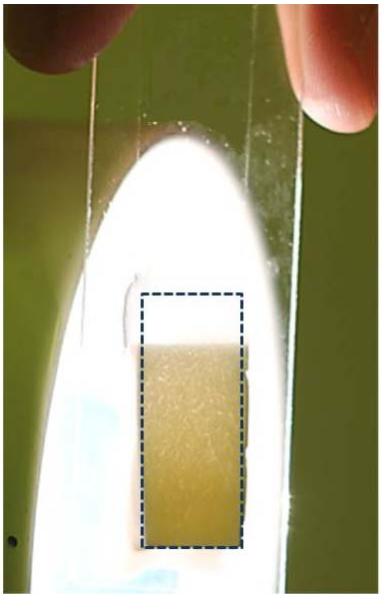

Figure 7: Example of HA particle gradient obtained at the end of the gelation process. In this example the HA particles were suspended in a 5% w/v gelatin solution with a 0.037 volume fraction

Gelatin-HA FGMs obtained using this technique can be covalently cross-linked using chemical agents (such as glutaraldehyde) and then freeze-dried to get a stable *off-the-shelf* scaffold for tissue engineering applications.

5 Conclusion

Continuous Functionally Graded Scaffolds (FGSs) were fabricated using gravitational sedimentation of discrete solid particles within a viscous fluid phase. In particular HA particle gradients were obtained by controlling the dynamic viscosity of a gelatin solution during its gelation process. As a result, when gelatin is completely gelled (using thermal gelation process), HA particles do not move from their given position: in this way tailored and stable HA particle gradients within a gelatin phase are obtained. With this novel approach we propose an alternative

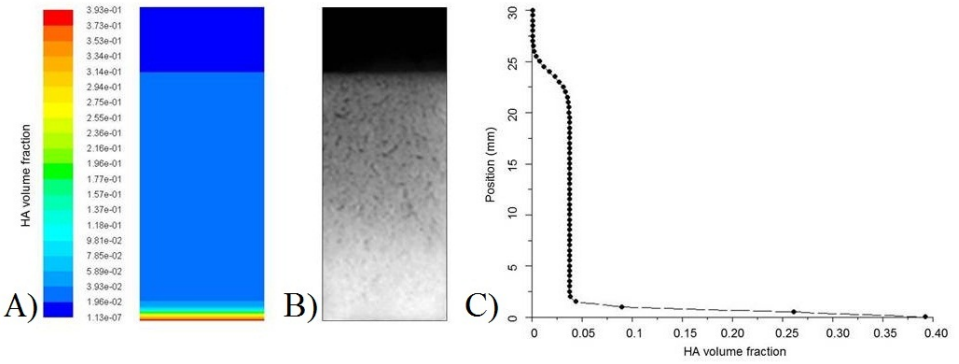

Figure 8: Comparison between the solution of the time-dependent viscosity CFD model and the corresponding experimental result at the end of the gelation of the fluid phase. A) CFD model HA volume fraction surface plot, B) experimentally obtained particle gradient, C) computed HA volume fraction plotted along the central vertical line of the parallelepiped cross-section shown in A.

and well-controlled technique to design and fabricate FGSs, overcoming problems related to discrete gradient scaffolds, e.g. impairment of pore interconnection and delamination between layers due to stress concentration.

CFD models are used to overcome the trial-and-error experimental approach, to predict and control particle gradient profiles in a fluid domain. Two-phase sedimentation models (primary fluid phase with constant and temperature/time variant dynamic viscosity) were solved to predict particle gradients. CFD model results were experimentally validated; confirming that HA particles can retain their position after the gelation of the fluid phase.

This simple and elegant approach can be used to design and control continuous graded materials and scaffolds with the minimum of equipment. Since composition gradients can be turned into pore size or porosity gradients, computational models can be further used to control pore size or porosity of a FGM. If desired more complex structures, which can be eventually used with RP systems to manufacture FGSs can be also designed. Merging CFD models with CAD and RP applications, the manufacturing of FGSs with biologically and physiologically relevant gradients can be applied to TE, as well as other fields. In TE they are of particular interest because tissues/organs exhibit gradients across a spatial volume. Therefore the investigation of the sedimentation process in two or more phase systems is useful to realise continuous graded scaffolds which mimic and fulfil the biological and mechanical requirements of the target tissue.

Nomenclature

Symbols are listed in order of appearance within equations shown in the paper.

α_q	$\boldsymbol{q}^{th}$ phase volume fraction
ρ_q	$\boldsymbol{q}^{th}$ phase density
$\vec{v}_q$	$\boldsymbol{q}^{th}$ phase velocity
$\dot{m}_{pq}$	mass transfer from phase $\boldsymbol{p}$ to phase $\boldsymbol{q}$
S_q	$\boldsymbol{q}^{th}$ phase source term
p	pressure (shared by all phases)
$\bar{\bar{\tau}}_q$	$\boldsymbol{q}^{th}$ phase stress-strain tensor
$\vec{g}$	acceleration due to gravity
$\vec{R}_{pq}$	interphase force
$\vec{v}_{pq}$	interphase velocity
$\vec{F}_q$	external body force
$\vec{F}_{lift,q}$	lift force
$\vec{F}_{vm,q}$	virtual mass force
μ_q	$\boldsymbol{q}^{th}$ phase shear viscosity
λ_q	$\boldsymbol{q}^{th}$ phase bulk viscosity
K_{pq}	interphase momentum exchange coefficient
$\bar{\bar{I}}$	identity tensor
d_s	$\boldsymbol{s}^{th}$ solid phase particle diameter
Re_s	relative Reynolds number
$v_{r,s}$	terminal velocity correlation for the solid phase
e_{ls}	coefficient of restitution
$C_{fr,ls}$	friction coefficient between the l^{th} and s^{th} solid particles
$g_{0,ls}$	radial distribution coefficient

References

Adachi, T., Osako, Y., Tanaka, M., Hojo, M. and Hollister, S. J. (2006): Framework for optimal design of porous scaffold microstructure by computational simulation of bone regeneration, *Biomaterials*, vol. 27, no. 21, pp. 3964–3972.

Batchelor G.K. (1972): Sedimentation in a dilute dispersion of spheres, *J. Fluid Mech*, vol. 52, no. 2, pp. 245-268.

Dalla Valle J. M. (1948): *Micromeritics*, Pitman, London.

Ding J. and Gidaspow D. (1990): A Bubbling Fluidization Model Using Kinetic Theory of Granular Flow, *AIChE J.*, vol. 36, no. 4, pp. 523–538.

Dullien F.A.L. (1992): *Porous Media. Fluid Transport and Pore Structure.* 2nd edition, Academic Press Inc.

Fels IG. (1964): Hydration and density of collagen and gelatin. *J Appl Polym Sci*, vol. 8, no. 4, pp. 1813–24.

Ford R.G., Miyamoto Y. and Nogata F. (1999a): In: Miyamoto Y., Kaysser W.A., Rabin B.H., Kawasaki A. and Ford R.G., *Functionally Graded Materials: Design, Processing and Applications*. Kluwer Academic Publishers, Boston, pp. 7-28.

Ford R.G., Miyamoto Y., Rabin B.H. and Williamson R.L. (1999b): In: Miyamoto Y., Kaysser W.A., Rabin B.H., Kawasaki A. and Ford R.G., *Functionally Graded Materials: Design, Processing and Applications*. Kluwer Academic Publishers, Boston, pp. 29–62.

Garside J. and Al-Dibouni M. R. (1977): Velocity-Voidage Relationships for Fluidization and Sedimentation, *I&EC Process Des. Dev.*, vol. 16, no. 2, pp. 206–214.

Hollister, S. J. (2005): Porous scaffold design for tissue engineering, *Nat. Mater.*, vol. 4, pp. 518–524.

Hollister, S. J., Maddox, R. D. and Taboas, J. M. (2002): Optimal design and fabrication of scaffolds to mimic tissue properties and satisfy biological constraints, *Biomaterials*, vol. 23, no. 20, pp. 4095–4103.

Hutchmacher, D. W. & Cool, S. (2007): Concepts of scaffold-based tissue engineering-the rationale to use solid free-form fabrication techniques, *J. Cell Mol. Med.*, vol. 11, no. 4, pp. 654–669.

Kalita S.J., Bose S., Bandyopadhyay A. and Hosick, H.L. (2003): Development of controlled porosity polymerceramic composite scaffolds via fused deposition modelling, *Materials Science and Engineering C*, vol. 23, no. 5, pp. 611–620.

Klein T.J., Chaundhry M., Bae W.C. and Sah R.L. (2007): Depth-dependent biomechanical and biochemical properties of fetal, newborn, and tissue-engineered articular cartilage, *Journal of Biomechanics*, vol. 40, no. 1, pp. 182-190.

Lun C. K. K., Savage S. B., Jeffrey D. J., and Chepurniy N. (1984): Kinetic Theories for Granular Flow: Inelastic Particles in Couette Flow and Slightly Inelastic Particles in a General Flow Field, *J. Fluid Mech.*, vol. 140, pp. 223–256.

Miot S., Woodfield T., Daniels A.U., Suetterlin R., Peterschmitt I., Heberer M., Blitterswijk C.A.V., Riesle J. and Martin I. (2005): Effects of scaffold composition and architecture on human nasal chondrocyte redifferentiation and cartiloginous matrix deposition, *Biomaterials*, vol. 26, no. 15, pp. 2479-2489.

Ogawa S., Umemura A., and Oshima N. (1980): On the Equation of Fully Fluidized Granular Materials. *J. Appl. Math. Phys.*, vol. 31, no. 4, pp. 483- 493.

Oh S.H., Park I.K., Kim J.M. and Lee J.H. (2007): In vitro and in vivo char-

acteristics of PCL scaffolds with pore size gradient fabricated by a centrifugation method, *Biomaterials*, vol. 28, no. 9, pp. 1664–1671.

Richardson J. R. and Zaki W. N. (1954): Sedimentation and Fluidization: Part I. *Trans. Inst. Chem. Eng.*, vol. 32, pp. 35–53.

Salem A.K., Stevens R., Pearson R.G., Davies M.C., Tendler S.J.B., Roberts C.J., Williams P.M. and Shakesheff K.M. (2002): Interactions of 3T3 fibroblast and endothelial cells with defined pore features, *Journal of Biomedical Materials Research*, vol. 61, no. 2, pp. 212-217.

Sherwood J.K., Riley S.L., Palazzolo R., Brown S.C., Monkhouse D.C., Coates M., Griffith L.G., Landeen L.K. and Ractliffe A. (2002): A three-dimensional osteochondral composite scaffold for articular cartilage repair, *Biomaterials*, vol. 23, no. 24, pp. 4739-4751.

Smith, M. H., Flanagan, C. L., Kemppainen, J. M., Sack, J. A., Chung, H., Das, S., Hollister, S. J. & Feinberg, S. E. (2007): Computed tomography-based tissue-engineered scaffolds in craniomaxillofacial surgery, *Int. J. Med. Robot.*, vol. 3, no. 3, pp. 207–216.

Song C., Wang P. and Makse H.A. (2008): A phase diagram for jammed matter, *Nature*, vol. 453, no. 7195, pp. 629–632.

Sun T., Norton D., Ryan A.J., MacNeil S. and Haycock J.W. (2007): Investigation of fibroblast and keratinocyte cell-scaffold interactions using a novel 3D cell culture system, *Journal of Materials Science: Materials in medicine*, vol. 18, no. 2, pp. 321-328.

Syamlal M. (1987): *The Particle-Particle Drag Term in a Multiparticle Model of Fluidization.* National Technical Information Service, Springfield, VA. DOE/MC/21353-2373, NTIS/DE87006500.

Syamlal M. and O'Brien T. J. (1989): Computer Simulation of Bubbles in a Fluidized Bed, *AIChE Symp. Series*, vol. 85, pp. 22–31

Syamlal M., Rogers W., and O'Brien T. J. (1993): *MFIX Documentation: Volume 1, Theory Guide*. National Technical Information Service, Springfield, VA. DOE/METC-9411004, NTIS/DE9400087.

Tampieri A., Celotti G., Sprio S., Delcogliano A., Franzese S. (2001): Porosity-graded hydroxyapatite ceramics to replace natural bone, *Biomaterials*, vol. 22, no. 11, pp. 1365–1370.

Tirella A., Vozzi F., Vozzi G. and Ahluwalia A. (2011): PAM2 (Piston Assisted Microsyringe): A New Rapid Prototyping Technique for Biofabrication of Cell Incorporated Scaffolds, *Tissue Engineering Part C: Methods*, vol. 17, no. 2, pp. 229-237.

Van Cleynenbreugel, T., Van Oosterwyck, H., Vander Sloten, J. & Schrooten, J. (2002): Trabecular bone scaffolding using a biomimetic approach, *J. Mater. Sci. Mater. Med.*, vol. 13, no. 12, pp. 1245–1249.

Vozzi G. and Ahluwalia A. (2007): Microfabrication for tissue engineering: rethinking the cells-on-a scaffold approach, *Journal of Materials Chemistry*, vol. 17, no. 13, pp. 1248–1254.

Werner J., Linner-Krcmar B., Friess W. and Greil P. (2002): Mechanical properties and in vitro cell compatibility of hydroxyapatite ceramics with graded pore structure. *Biomaterials*, vol. 23, no. 21, pp. 4285–4294.

Woodfield T.B.F., Malda J., de Wijn J., Peters F., Riesle J. and van Blitterswijk C.A. (2004): Design of porous scaffolds for cartilage tissue engineering using a threedimensional fiber-deposition technique, *Biomaterials*, vol. 25, no. 18, pp. 4149–4161.

Zeschky J., Hofner T., Arnold C., Weissmann R., BahloulHourlier D., Scheffler M. and Greil P. (2005): Polysilsesquioxane derived ceramic foams with gradient porosity, *Acta Materialia*, vol. 53, pp. 927–937.